Bioactive Materials 24 (2023) 112–123

Contents lists available at ScienceDirect

Bioactive Materials

journal homepage: www.keaipublishing.com/en/journals/bioactive-materials

A sandwiched patch toward leakage-free and anti-postoperative tissue adhesion sealing of intestinal injuries

Wei Yang [a,b], Chengkai Xuan [a,b,f], Xuemin Liu [a,b], Qiang Zhang [a,b], Kai Wu [e], Liming Bian [a,c,d,e,**], Xuetao Shi [a,b,c,d,*]

[a] National Engineering Research Centre for Tissue Restoration and Reconstruction, South China University of Technology, Guangzhou, 510006, China
[b] School of Materials Science and Engineering, South China University of Technology, Guangzhou, 510640, China
[c] Key Laboratory of Biomedical Engineering of Guangdong Province, South China University of Technology, Guangzhou, 510006, China
[d] Key Laboratory of Biomedical Materials and Engineering of the Ministry of Education, South China University of Technology, Guangzhou, 510006, China
[e] School of Biomedical Sciences and Engineering, South China University of Technology, Guangzhou International Campus, Guangzhou, 511442, China
[f] Guangzhou Soonheal Medical Technology. Co, Ltd, Guangzhou, 510230, China

ARTICLE INFO

Keywords:
Trilayer patch
Bioadhesives
Preventing postoperative adhesion
Antiadhesion
Intestinal injuries

ABSTRACT

Ideal repair of intestinal injury requires a combination of leakage-free sealing and postoperative antiadhesion. However, neither conventional hand-sewn closures nor existing bioglues/patches can achieve such a combination. To this end, we develop a sandwiched patch composed of an inner adhesive and an outer antiadhesive layer that are topologically linked together through a reinforced interlayer. The inner adhesive layer tightly and instantly adheres to the wound sites via -NHS chemistry; the outer antiadhesive layer can inhibit cell and protein fouling based on the zwitterion structure; and the interlayer enhances the bulk resilience of the patch under excessive deformation. This complementary trilayer patch (TLP) possesses a unique combination of instant wet adhesion, high mechanical strength, and biological inertness. Both rat and pig models demonstrate that the sandwiched TLP can effectively seal intestinal injuries and inhibit undesired postoperative tissue adhesion. The study provides valuable insight into the design of multifunctional bioadhesives to enhance the treatment efficacy of intestinal injuries.

1. Introduction

The intestine digests food, absorbs water and exhausts waste from the body. Intestinal injuries frequently occur due to intestinal cancer, local lesions or any activity that causes a serious blow to the abdomen [1–4]. Ideal treatment of intestinal injuries should bear two features: (i) sealing of the injury defect should be free of leakage; otherwise, the material inside the intestine will leak into the abdomen, causing a serious and possibly life-threatening infection [5–8], and (ii) postoperative adhesions should be sufficiently well suppressed to avoid acute intestinal and bowel obstructions, among other complications [9–11]. Unfortunately, none of the current surgical repair strategies for intestinal injuries can simultaneously achieve leakage-free and anti-postoperative sealing performance.

Sutures are commonly adopted to execute sealing for intestinal trauma through hand-sewn closures of intestinal injuries (Fig. 1a) [5]. Tissue damage from sutures is inevitable due to needle piercing, which frequently results in anastomotic leaks as well as complications, including infection, sepsis, and even death [12,13]. Furthermore, suturing is a time-consuming process and thus increases the risk of secondary inflection due to the prolonged exposure time of the injured intestine [14,15]. As an alternative to sutures, bioglues (i.e., Coseal, fibrin glue and so on) have emerged as a time-saving sealing treatment for intestinal repair [16–19]. However, most bioglues are in a liquid state when delivered to the would sites; thus, they can be diluted or even washed off by a large amount of tissue fluid seeping from the damaged intestine, limiting the sealing efficiency for intestinal defects [20,21].

In addition to bioglues, solid-state adhesive patches have

Peer review under responsibility of KeAi Communications Co., Ltd.
* Corresponding author. School of Materials Science and Engineering, South China University of Technology, Guangzhou, 510640, China.
** Corresponding author. National Engineering Research Centre for Tissue Restoration and Reconstruction, South China University of Technology, Guangzhou, 510006, China.
E-mail addresses: bianlm@scut.edu.cn (L. Bian), shxt@scut.edu.cn (X. Shi).

https://doi.org/10.1016/j.bioactmat.2022.12.003
Received 10 August 2022; Received in revised form 1 December 2022; Accepted 2 December 2022

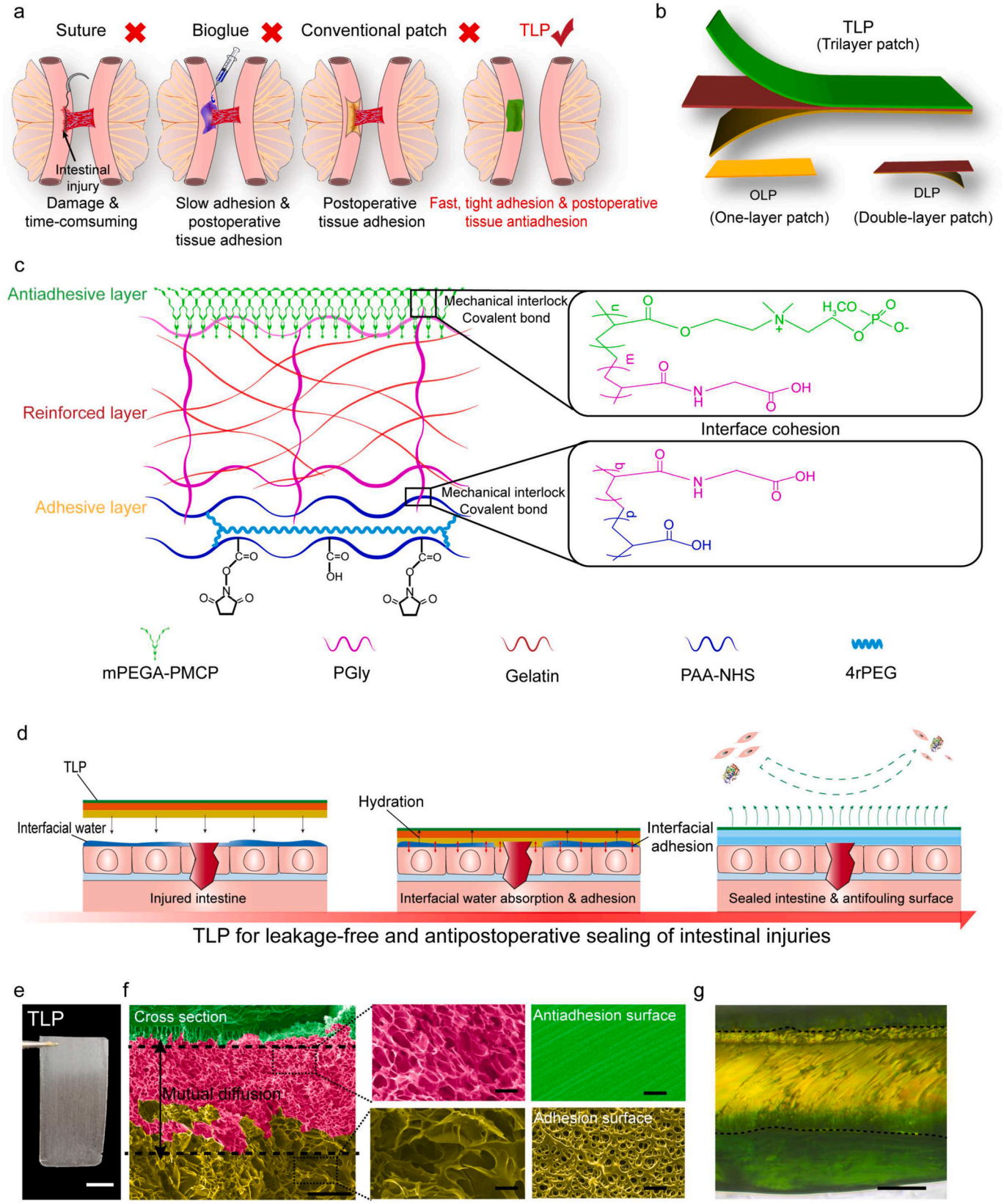

Fig. 1. Design and mechanism of the sandwiched patch. (a) Schematic illustrations of different sealant applications for intestine repair. (b) Schematic illustrations of the structure design of the TLP. (c) Schematic overview of the internal molecular combination and interfacial action in the trilayer sandwiched patch. (d) Schematic illustrations of the adhesion mechanism of the TLP. (e) Photograph of the dry TLP. Scale bar: 1 cm. (f) Scanning electron microscope (SEM) images of the cross section and surface morphologies of the TLP. The false color on the images was used for better distinction. Scale bars: 50 μm (g) Cross-section image of TLP labeling with different dyes on the TLP by fluorescence microscope observation. Scale bar: 50 μm mPEGA, methoxy poly(ethylene glycol) monoacrylate; PMCP, poly[2-(meth-acryloyloxy)ethyl choline phosphate]; PGly, poly(glycine); 4rPEG, 4-arm PEG amino.

demonstrated superb performance in sutureless repair of damaged tissues [5,22,23]. In a pioneering work by Zhao's group, dry adhesive tape was directly employed to seal heart defects within 5 s [24]. Zhu et al. prepared hydrogel bioadhesives for promoting oral mucosal wound healing [25]. Despite progress, double-sided bioadhesives may still lead to undesired postsurgical adhesion owing to their indiscriminate adhesion to surrounding normal intestinal tissue, and such postoperative adhesion cannot be thoroughly addressed by simply modifying the backside of the patch with nonadhesive groups [26–29]. Furthermore, most bioadhesives composed of bioactive groups can adsorb proteins and cells, which subsequently promote inflammation and fibrosis to cause postoperative tissue adhesion [30–33]. Overall, it is desired yet challenging to fabricate a sealant for intestinal injury with a combination of timely sealing, single-side adhesion, and anti-tissue adhesion.

To address these challenges, we conceived a three-layer sandwiched patch composed of an adhesive bottom layer, a reinforced interlayer and an antiadhesive top layer (Fig. 1b). Adjacent layer interfaces are tightly connected by covalent bonds and mechanical interlocking of entangled polymers. These integrated layers synergistically function to render leakage-free and anti-postoperative repairs for intestinal injury. The adhesive layer specifically and rapidly adhered to the wet tissue surface based on covalent anchoring (Fig. 1c–d). The reinforced layer aids the congruent and robust attachment of patches on intestines. The top layer inhibits protein and cell adhesion to prevent postoperative adhesion. Such a trilayer patch (TLP) possesses a unique combination of instant wet adhesion, high mechanical strength and biological inertness. To this end, the TLP can effectively seal the injury without causing undesired postoperative tissue adhesion, as demonstrated in both rat and pig experiments. In addition, our data further revealed that the outstanding tissue antiadhesion capability of the sandwiched patch can be attributed to the significant inhibition of postoperative inflammation and fibrosis. This research thus establishes a potential strategy to enhance the treatment efficacy of intestinal injuries in the clinic.

2. Materials and methods

2.1. Bioadhesive patch fabrication

The TLP was prepared by the combination of an adhesive layer, a reinforced layer and an antiadhesive layer based on free radical copolymerization. The adhesive layer was first prepared by UV-curing for 5 min. The prepolymer solution for the adhesive layer, including acrylic acid (AA) with a concentration of 30 wt%, acrylic acid N-hydroxysuccinimide ester (AA-NHS) with a concentration of 1 wt%, 4rPEG with a concentration of 4 wt%, PEGDA (*Mn* 2000) with a concentration of 0.06 wt% and α-ketoglutaric acid with a concentration of 0.1 wt%, was added to a square polytetrafluoroethylene mold with a depth of 0.5 mm, and the solution was dried in an oven (50 °C, 2 min). Then, the prepolymer solution for the reinforced layer mainly composed of gelatin (3%, w/w), N-acryloyl-2-glycine (AGly, 27 wt%) and α-ketoglutaric acid (1%, w/w) was UV cured on the top surface of the adhesive layer (365 nm, 5 min) and dried in an oven (50 °C, 2 min). The antiadhesion layer was prepared by the same method above on the surface of the reinforced layer using the prepolymer solution mainly composed of mPEGA (20%, w/w) and MCP (100%, w/w) in deionized water; however, the curing time was adjusted to 30 min. Then, the patch was dried in an oven (50 °C, 2 min), removed from the model and stored at −20 °C before use. During the preparation of the TLP, the volume ratio of the adhesive layer to the reinforced layer to the antiadhesive layer was 2/4/1. A size of 4 cm × 0.75 cm × 200 μm for TLP was showcased in further adhesion experiments unless specified. A one-layer patch (OLP) and a double-layer patch (DLP) were prepared using the same method as TLP for further control study.

2.2. Adhesive properties of TLP

Fresh intestinal tissue was cleaned to remove the residual fat, covered with an excess of PBS solution spray and sealed in plastic bags to prevent degradation and dehydration. To detect the adhesive performance, the tissue surface was adhered by the adhesive side of the patch sample with 5 s of pressing under 1 kPa pressure, and stiff backings on the other size using cyanoacrylate glue before performing 180° peeling, tensile and lap-shear tests at a continuous rate of 30 mm min^{-1}. Interfacial toughness was examined by 180° peeling tests. The adhesion strength of patch samples was detected after hydration and swelling of patches adhering to tissue for 2 min. Covalent bond adhesion was performed by immersing the TLP with and without the addition of AA-NHS in aqueous solution that contained 1 mg/mL green fluorescent microspheres polymethyl methacrylate with -NH_2. After 5 min, these samples were gently removed, washed using deionized water, and observed under a fluorescence microscope.

2.3. Mechanical properties of TLP

The sample was cut into a dogbone shape (40 × 7.5 × 1 mm^3) for the stress–strain test and circle tensile test, which were performed 10 times to achieve 100%. To evaluate the tough adhesion and reliable mechanical strength of the TLP that was not broken by intestinal pressure, a burst pressure test was conducted with the normal intestine inner pressure as the contrast value. Herein, a penetrable hole (10 mm in diameter) was created on the pig intestine; then, one end of the intestine was closed using operating scissors, and the other end was connected to the pressure pump. Next, the hole was sealed by a square TLP. Finally, the syringe pump with PBS solution was pumped with continuous speed, and the highest value was recorded when the sample broke.

2.4. In vitro biocompatibility evaluation

Rat fibrocytes were used to evaluate the in vitro cytocompatibility of TLP. Leachate from the TLP that was immersed in PBS for 24 h was cocultured with cells and further evaluated with a live/dead cell kit. Briefly, the cells (2 × 10^4/well) were seeded in 24-well plates, and then cocultured with the samples in a standard incubator for 1, 3 and 5 days. Two microliters of ethidium homodimer-1 and 0.5 μL of calcein acetomethoxy within 1 mL of DEME medium were used to stain the cells, after being fixed first using 4% paraformaldehyde for 30 min. A fluorescence microscope (Nikon Ti2, Japan) was used to image the stained cells.

Cytotoxicity was analyzed by a cell counting kit (CCK-8). Briefly, fibrocytes (1 × 10^3/well) were seeded in 96-well plates and cocultured with samples. CCK-8 solution was used for detection according to the instruction manual at the preset time. The absorbance value at 450 nm was recorded to assess the cytotoxicity by a microplate reader (BioTek Corporation imaging reader, USA).

2.5. In vitro and in vivo biodegradability

The in vitro biodegradation tests of the TLP were conducted using protease degradation. One hundred milliliters of PBS with 5 mg collagenase was chosen as the degradation medium. The samples of the TLP cutting to a square size (25 mm × 25 mm × 1 mm) were immersed in 15 mL of the prepared degradation medium and incubated at 37 °C with shaking at 60 r.p.m. At the preset time, the samples were removed from the incubation medium, exhaustively washed with deionized water and lyophilized. Weight loss was determined as the percentage ratio of the mass of the lyophilized sample at each time interval, normalized by the dry mass of the original lyophilized sample.

To further evaluate the *in vivo* biodegradability, the TLP was cut into a square size (25 mm × 25 mm × 1 mm) and implanted into the subcutaneous tissue of rats. The rats were sacrificed at week 2 and week 4, and then the residue sample was washed with deionized water and

weighed. The responding blood and key organ tissue were detected and analyzed.

2.6. Measurement of nonspecific protein adsorption

The samples were rinsed with bovine serum albumin (BSA), fibrin, collagen, and serum solution (2 mg/mL) in a 24-well plate. After incubation at 37 °C for 2 h, the samples were gently removed from the protein solution and washed five times with deionized water to remove the loosely adsorbed protein on the surface. Then, those samples were immersed in 1 mL of fresh deionized water and subjected to sustained ultrasound cleaning for 10 min to knock off the proteins that were firmly adsorbed on the hydrogel. The adsorbed protein was quantified using the micro-BCA kit according to the manufacturer's instructions. Fluorescein isothiocyanate (FITC)-labeled BSA and collagen were used for qualitative detection by the same experimental procedure described above. The samples that absorbed protein were observed by inverted fluorescence microscopy.

2.7. In vivo biological adhesive and antiadhesion capacity evaluation of rats and pigs

Eight-week-old male SD rats were used to create small intestine injury models with an incision of 5 mm length, and 6-month-old male mini-pigs were used to construct a small intestinal injury model with an incision 10 mm in length. In the rat operative antiadhesion model, DLP and OLP were chosen as the control groups to seal the incision, and TLP was chosen as the experimental group. The commercial Coseal adhesive and Interceed film that contained an additional suture fixed to the tissue were considered to be the control group that sealed the incision in the pig evaluation model. All surgical procedures were performed under sterile conditions consistent with the Ethical Committee regulations (No. HTSW210816) of Huateng Biopharmaceutical Technology Co., Ltd in Guangzhou, China. The rats were sacrificed immediately at 1 week and 2 weeks after the operation. Hematoxylin and eosin (H&E), Masson and immunofluorescence staining were used for tissue analysis. The pigs were sacrificed at 2 weeks after the operation to collect tissue samples for pathological verification.

2.8. Statistical analysis

All data are expressed as the means ± standard deviations (SD) and were analyzed using one-way ANOVA. A p value < 0.05 was considered statistically significant. $^{*}p < 0.05$, $^{**}p < 0.01$, $^{***}p < 0.001$.

3. Results and discussion

3.1. Design of the sandwiched TLP

As a proof of concept, the TLP was assembled *via* layer-by-layer polymerization methods (Fig. S1) and was hierarchically optimized for a more stable structure, as described in the supporting information (Figs. S2–S8). For comparison and to highlight the crucial roles of the sandwiched structure and each layer, we also prepared an OLP and DLP, in which the OLP comprised only the adhesive layer and the DLP was composed of the adhesive layer and reinforced interlayer and no antiadhesive layer. The TLP was semitransparent and did not contain residuals of adverse acrylic acid monomers (Fig. 1e and Fig. S9). The molecular structure of the TLP was proven by Fourier transform infrared spectroscopy (FTIR) and X-ray photoelectron spectroscopy (XPS) (Fig. S10). Furthermore, the TLP can withstand gentle pulling, bending, wrenching and rolling after absorbing water (Movie S1 and Fig. S11). According to scanning electron microscope (SEM) examinations of the cross section of this patch, it was confirmed that the three layers in the TLP welded to each other *via* mutual diffusion (Fig. 1f). This sufficiently interpenetrated interface was further accessed by labeled layers, indicating the formation of a stable structure (Fig. 1g).

csSupplementary video related to this article can be found at https://doi.org/10.1016/j.bioactmat.2022.12.003

Interestingly, the pore size gradually increases from the antiadhesive layer to the adhesive layer without boundaries, indicating that the reinforced middle matrix formed a stable combination with the adjacent layers based on the interfacial covalent bone and mechanical interlocking. Additionally, the surface of the antiadhesive layer is dense and smooth, benefiting antiadhesion. The surface of the adhesive layer is highly porous and rough, contributing to tissue adhesion. The morphology feature can be inferred that a high crosslinking density appeared in the thin antiadhesive layer based on a high content of MCP and mPEGDA; however, a low crosslinking density and hydrophilic matrix led to large pores.

The tensile strength of the TLP reaches 303 kPa, which is one order of magnitude higher than that of the OLP (≈21 kPa). Interestingly, the TLP can successfully hold a weight of 500 g, but the OLP and the control group that was combined by the adhesive layer and antiadhesive layer broke under the same loading (Fig. S12a). The TLP exhibits outstanding resilience, demonstrating the capability to be restored from deformation even after hundreds of loading–unloading cycles (Fig. S12b). Rheological tests further confirmed the improved resilience of the TLP compared to the OLP (Fig. S13a). In addition, increasing the shear rate reduces the viscosity, which can be attributed to the shear-induced breaking of dynamic bonds, such as hydrogen bonds [34].

3.2. Adhesive performance

Next, we examined the adhesion performance of the TLP in vitro. The capacity of the TLP to absorb water at the tissue interface plays a key role in wet interface adhesion. After being hydrated in water, the antiadhesive layer becomes smoother. In contrast, the roughness of the adhesive layer increases upon water absorption, and increased roughness was reported to enhance the seamless contact between bioadhesives and the tissue (Fig. 2a) [16,45,46]. We infer that a thin antiadhesive layer forms a hydration layer on the surface and that a thick adhesive layer can rapidly absorb the interfacial water based on the abundant pore structure. In addition, the TLP exhibited a swelling ratio of 1600% and 4-fold volume expansion in a body-liquid mimic (Fig. S14), which confirms that the TLP can effectively absorb interfacial water to promote tissue adhesion. Notably, we hardly observed delamination in the swelling state, which will benefit the subsequent application of intestine adhesion.

To comprehensively assess the adhesion performance of the TLP under various deformation modes, lap-shear, tensile and 180° peel tests between patches and intestines were performed (Fig. 2b–d). For the TLP, tight (with an interfacial toughness of ~84 J m^{-2}) and tough (with a shear strength of ~53 kPa and tensile strength of ~118 kPa) adhesion values were greater than those of the OLP. To assess adhesion to the intestine under wet conditions, the intestine sealed with the TLP was immersed in deionized water for different times. The adhesion strength changed from 38.7 to 24.1 kPa after soaking in water for 0.5–24 h (Fig. 2e). To confirm the successful and effective adhesion mode, the adhesion strength test of TLP adhered to wet intestine over the changed pressing time was conducted, and maximal adhesion strength was achieved under the continuous pressure of 1 kPa for 5 s (Fig. S15). The tight adhesion to tissue underwater was due to covalent bonding *via* -NHS chemistry (Fig. S16). The adhesion strength showed a slight decreasing tendency, which could be ascribed to the destruction of hydrogen bonds under abundant water. However, although it decreased, the final adhesion strength was still higher than that of most of the previous hydrogel adhesives (Fig. 2f). Moreover, the TLP showed entirely different adhesive properties of the two surfaces, and the antiadhesive surface showed negligible adhesion, indicating stable versatility (Fig. 2g). Burst pressure test results were obtained through the adherence of a patch to pig intestine tissue with a 5 mm hole under liquid

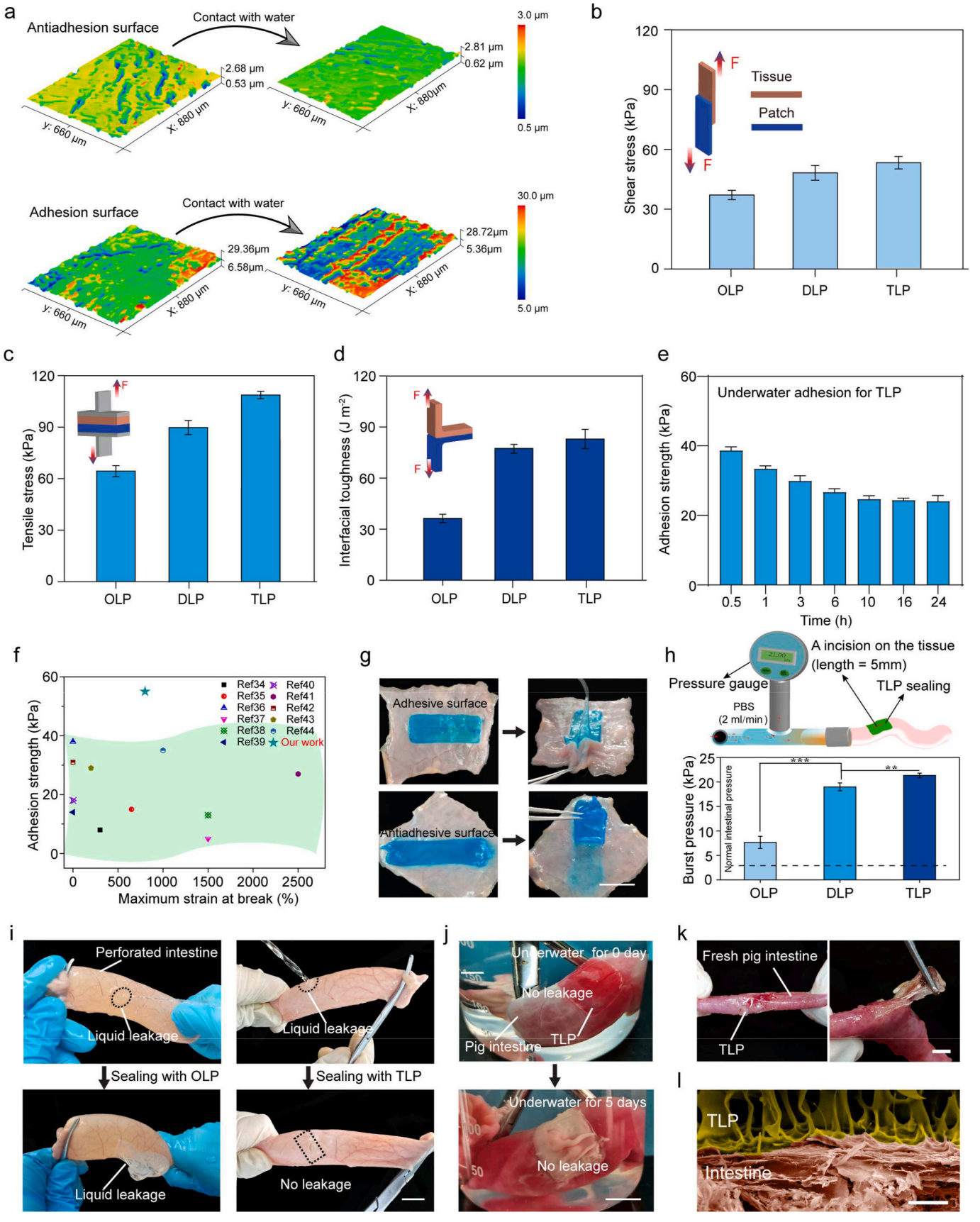

(caption on next page)

Fig. 2. TLP adhesion performance. (a) 3D contour images of the antiadhesion surface and adhesion surface of the dry TLP before and after contacting water. (b–d) Schematic illustrations of the adhesion tests through lap-shear, tensile and 180° peeling tests, respectively (n = 3). (e) The lap-shear adhesion strength of the TLP to a pig intestine after rinsing in water for the preset time interval (n = 3). (f) Comprehensive comparison between TLP and the reported adhesive hydrogels regarding the adhesion strength and fracture strain [34–44]. (g) Pictures showing the adhesion property of the adhesive surface and antiadhesive surface of the TLP labeled with blue dye for observation. Scale bar: 10 mm. (h) Schematic diagram of the designed setup for quantitative analysis of burst pressure (n = 3). (i) Comparison of adhesion strength between the OLP and TLP applied to a perforated intestine with water pressure. Scale bar: 10 mm. (j) Pictures showing the instant immersed adhesion of the TLP to the pig intestine under pumping water conditions with the addition of red dye to observe further leakage underwater. Scale bar: 10 mm. (k) Pictures showing the robust adhesion of the TLP to the fresh pig intestine. Scale bar: 10 mm. (l) The morphology of the interfacial adhesion state between the TLP and intestinal tissue by SEM observation. False color was used to achieve better observations. Scale bar: 50 μm $^{**}p < 0.01$, $^{***}p < 0.001$.

pressure, which instantly increased (Fig. 2h). The TLP showed a burst pressure of 21 kPa, approximately 2.7 times higher than that of the OLP. To determine the *in vivo* sealing performance, a 5 mm incision was created in vitro on the center of the pig intestine by pumping liquid with strong pressure, and the TLP successfully sealed the incision, but the OLP could not instantly seal the incision (Fig. 2i). Afterwards, the sealed pig intestine was pumped with a red dye solution, and no leakage was detected after the fifth day (Fig. 2j). Moreover, a more reliable adhesion simulation was investigated using the fresh pig intestine, and the TLP showed robust adhesion to the pig intestine (Fig. 2k). As shown in the SEM results (Fig. 2l), a tight combination between the TLP adhesive layer and intestine tissue surface formed.

3.3. Antifouling performance of the sandwiched patch

The adhesion of cells and proteins is closely related to the hydrophobic interaction of the patch surface (Fig. 3a) [47–53]. The antiadhesion surface of the sandwiched patch with a relatively smooth morphology had a low contact angle of approximately 16°, which resulted in hydrophilic performance. The ability of the TLP to resist fouling was further evaluated by detecting the resistance to cell attachment and nonspecific protein adsorption. TLP exhibited outstanding resistance to nonspecific protein absorption by observing FITC-labeled BSA and collagen absorption by fluorescence microscopy (Fig. 3b). The quantitative absorption test indicated that the absorbed BSA was 0.757 μg/cm^2 for OLP, 0.645 μg/cm^2 for DLP and 0.139 μg/cm^2 for TLP (Fig. 3c). The amount of absorbed collagen, which is an important protein that promotes cell adhesion, was 0.502 μg/cm^2 for OLP, 0.678 μg/cm^2 for DLP and 0.147 μg/cm^2 for TLP (Fig. 3d). The amount of absorbed fibrin, which is related to blood clotting and thrombosis formation, was 0.292 μg/cm^2 for OLP, 0.267 μg/cm^2 for DLP and 0.045 μg/cm^2 for TLP (Fig. 3e). The amount of absorbed serum, which acted as a complex mixture that promoted cell adhesion, was 0.6 μg/cm^2 for OLP, 1.26 μg/cm^2 for DLP and 0.246 μg/cm^2 for TLP (Fig. 3f). This superb antifouling performance is related to a tight hydration layer on the TLP surface [30,54,55], which may occur due to superhydrophilic moieties that exhibit a remarkably strong resistance to protein adhesion. The antifouling efficiency of TLP is superior to that of some individual antifouling biomaterials without tissue adhesion function as previously reported [10,11,29,55]. The capacity of blood to self-fuse was examined to stimulate the inevitable obstacles that occur when the TLP was applied *in vivo*. The antiadhesive layer showed remarkable resistance to the blood coating (Fig. S17).

During the intestine operation, the abdomen will inevitably be cut to cause rupture of the vein. In addition, abundant veins are distributed in intestinal tissue, and are easily broken after injury, and there is a high chance that human umbilical vein endothelial cells (HUVECs) will interact with implant biomaterials. Adhesion against L929 cells and HUVECs on the antiadhesive layer of the TLP was further evaluated (Fig. 3g). The cells were barely observed in the TLP at all times after cell seeding on the surface of different layers. In contrast, dense cells adhered to the surface of the OLP and DLP, indicating that the materials have a superb ability to prevent cell adhesion (Fig. 3h).

3.4. Biocompatibility and degradability of the sandwiched TLP

The outstanding cytocompatibility of the TLP was validated after 7 days of incubation with fibroblasts derived from mice (Fig. 4a–b). The in vitro degradation kinetics indicated that complete degradation occurred after one month (Fig. 4c). The *in vivo* degradation was monitored after the TLPs were subcutaneously implanted in rat models (Fig. 4d). The TLP was almost completely degraded within 2 weeks and vanished at the fourth week (Fig. 4e). The same and normal levels of red blood cell and monocyte concentrations were observed at all times. Despite the increase in white blood cell and neutrophil concentrations that was observed at the second week, the values were within normal concentration ranges and remained almost constant at the fourth week (Fig. 4f–g). No significant signs of inflammatory lesions or damage were observed in the key organs, indicating that the TLP has outstanding biocompatibility (Fig. 4h).

3.5. Injury sealing and tissue antiadhesion in a rat intestinal injury model

Encouraged by the favorable comprehensive properties, the versatile TLP was applied *in vivo* to prevent postoperative adhesion in a rat model, in which an intestinal sidewall injury was made with a 5 mm incision (Fig. 5a). An instant pressing process with approximately 1 kPa for 5 s was conducted on the TLP to promote interfacial water absorption to soften and improve the fast H-bone interaction between the adhesive and tissue. Furthermore, robust adhesion to the intestine was demonstrated *in vivo* under high internal pressure intervention through instant saline injection (Fig. S18 and Movie S2), which was advantageous for the TLP once the intestine expanded during digestion.

csSupplementary video related to this article can be found at https://doi.org/10.1016/j.bioactmat.2022.12.003

The antiadhesion effect of the TLP on the injured intestine was confirmed and scored at week 1 and week 2 according to the unified scoring criteria. At week 1, the nontreatment group was 3.1, the OLP was 3.8, the DLP was 2.2 and the TLP was 0.1 (Fig. 5c). A significant difference was observed between the no-treatment and DLP groups, demonstrating that an effective physical barrier from the injury sealant could slightly alleviate postoperative adhesion. We reasoned that complications can easily occur when the damaged intestine is sealed only by common bioadhesives due to leakage and indiscriminate adhesion from the surface layer [26,56–58]. At week 2, the untreated group scored 4.4 for the OLP, 3.4 for the DLP and 0.1 for the TLP. Except for the TLP, the surrounding circumjacent mesentery and surface of the damaged intestine wall were severely adhered due to invalid treatment (Fig. 5b and Fig. S19a). Afterwards, the degree of wound healing was evaluated, and the TLP exhibited the highest wound aggregation (Fig. S19b).

The pathological changes were analyzed through H&E and Masson staining as the intestine wall healed (Fig. 5d and Fig. S20). As shown in the H&E staining results, substantial formation of adhesion tissue and obvious inflammatory cells appeared on the intestine surface in the untreated, OLP and DLP groups at week 2. In the TLP group, there was a layer of new mesothelial cells that were restored in the injured position without visual tissue adhesion. Masson's trichrome staining results showed collagen deposition in the untreated, OLP and DLP groups, revealing that abundant fibroblast adhesion occurred. The TLP group had a similar collage structure to that of the normal group at week 2.

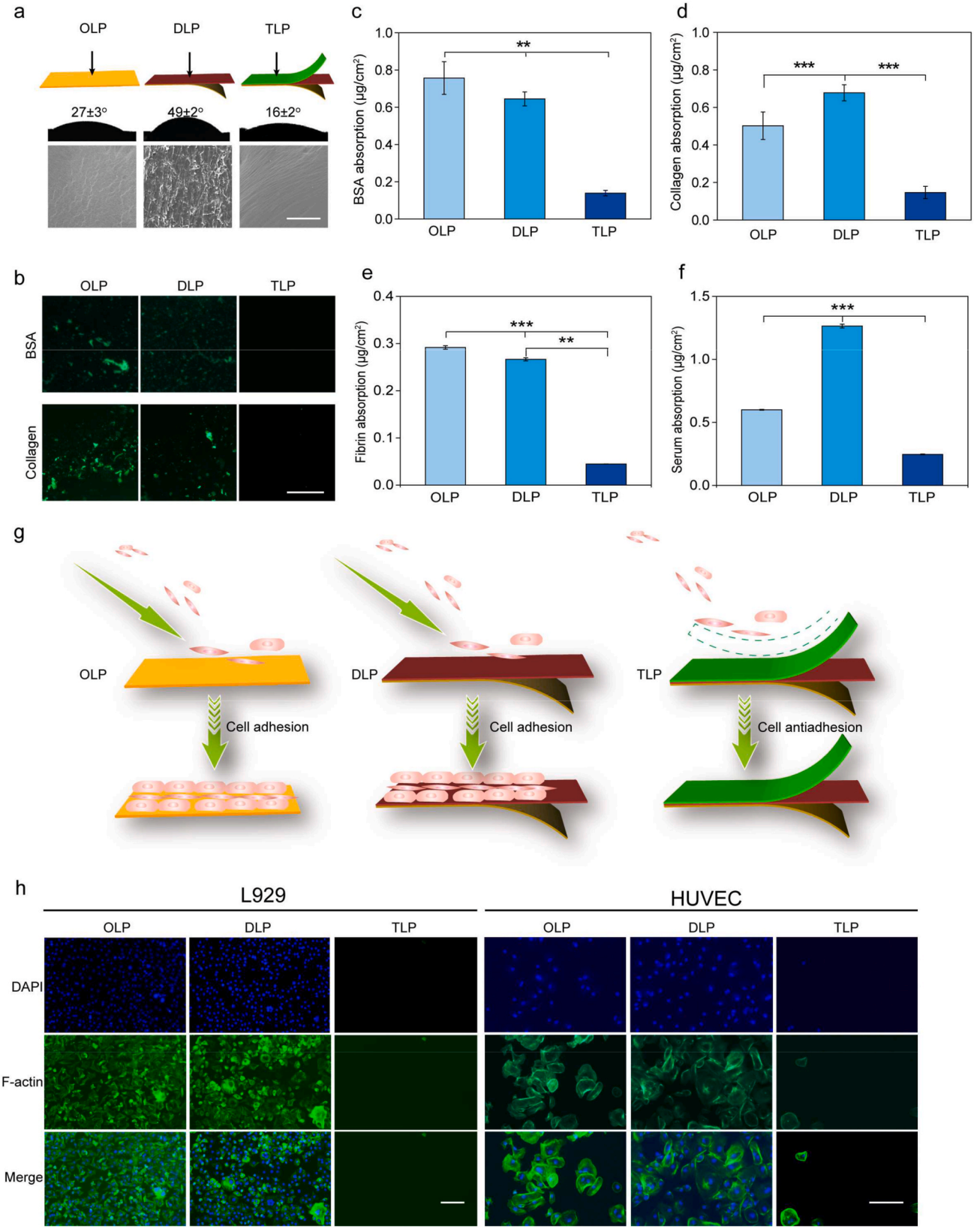

Fig. 3. Antifouling performance of the sandwiched patch. (a) Water contact angles and SEM observation morphology on the surface of three layers. Scale bar: 100 μm. (b) Fluorescence images of fluorescein isothiocyanate-labeled BSA and collagen absorption on the top surface of OLP, DLP and TLP. Scale bar: 100 μm. (c–f) Quantitative measurement of BSA, collagen, fibrin and serum absorption on the top surface of the OLP, DLP and TLP (n = 5). (g) Schematic illustrations of cell adhesion behaviors on the different surfaces of the sandwiched TLP. (h) L929 and HUVEC adhesion on the top surface of the OLP after seeding for 2 h. Scale bars: 100 μm $^{**}p < 0.01$, $^{***}p < 0.001$.

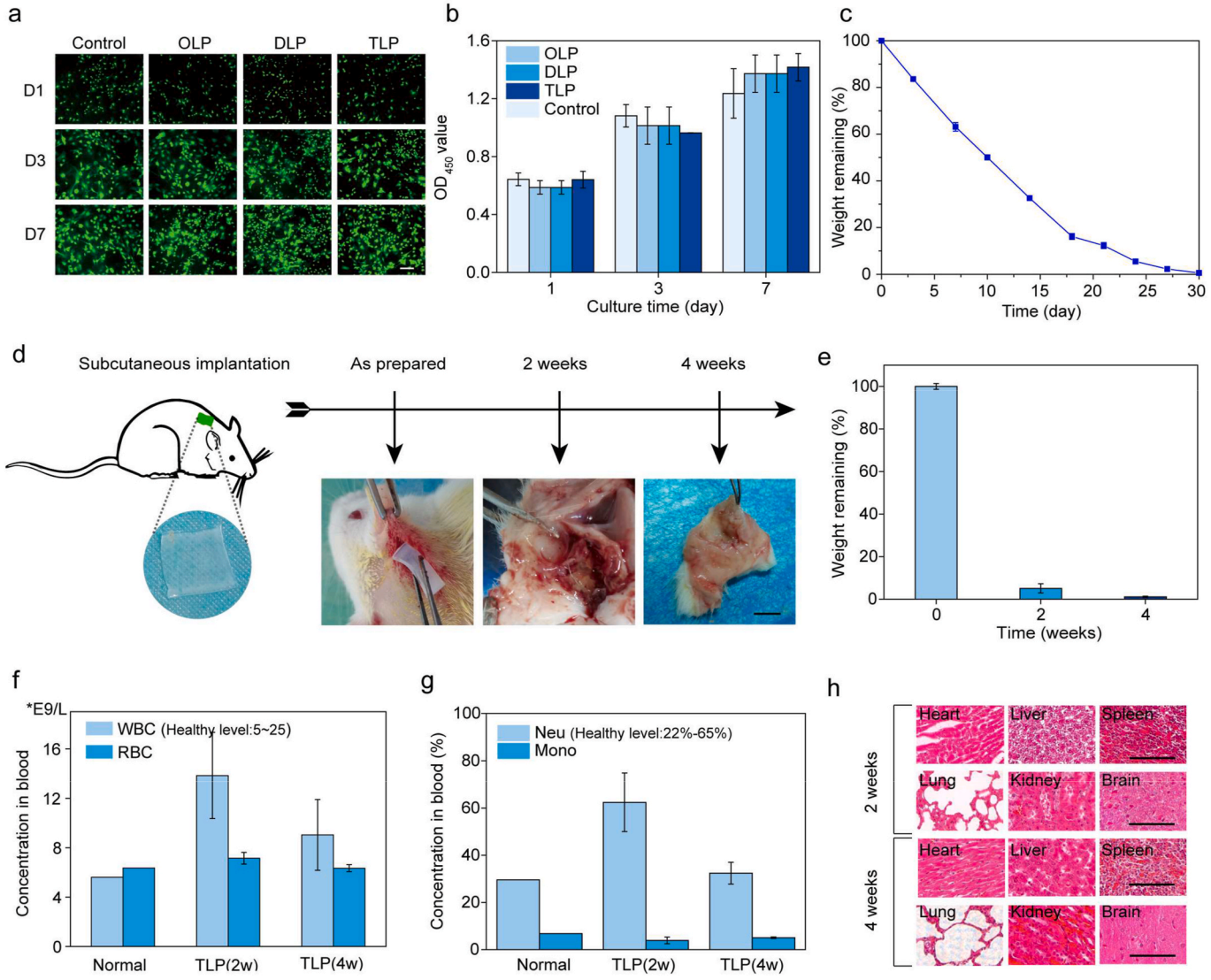

Fig. 4. In vitro and *in vivo* biocompatibility of the sandwiched patch. (a) Representative live/dead assay images and (b) fibroblast viability of OLP, DLP and TLP after 1, 3 and 7 days of culture. Scale bar: 100 μm (n = 5). (c) The in vitro degradation curve of the sandwiched patch in phosphate buffered saline (PBS) with protease at 37 °C. (d–e) *In vivo* degradation of the TLP in the subcutaneous tissue of rats for 2 and 4 weeks (n = 3). Scale bar: 1 cm. (f–g) TLP samples that were implanted *in vivo* resulted in an inflammatory response (n = 3). White blood cell (WBC), red blood cell (RBC), neutrophil (Neu), monocyte (Momo). (h) Key organ toxicities in the heart, liver, spleen, lung, kidney and brain at 2 and 4 weeks. Scale bars: 100 μm.

Moreover, the intestinal surface is damaged, and then the inflammatory response and the fibrosis process simultaneously occur locally. Inflammatory cells release proinflammatory cytokines such as interleukin-6 (IL-6), IL-1β, TNF-α and interleukin-1β. Moreover, TGF-β1 is regarded as the key fibrotic mediator during the tissue adhesion process. TNF-α not only accelerates blood coagulation and inflammation effects, but also decreases fibrinolysis by provoking the constant release of PI in the regulation of fiber deposition and reducing PA levels in the regulation of fiber degradation. The imbalance between the PI and PA is the pivotal sign for adhesion formation [59,60]. The levels of gene expression for IL-1β, IL-6 and TNF-α were pronouncedly downregulated in the TLP group compared to those in the control groups at 1 week or 2 weeks (Fig. 5e and Fig. S21). The levels of gene expression for TGF-1β, which promotes fibrosis, were downregulated and showed the lowest value among the three groups. The levels of PA and PI gene expression were disturbed in the OLP and no-treatment groups, leading to an abnormal balance level of fibrinolytic activity. In contrast, the expression levels in the TLP group exhibited a normal trend, with downregulated PI and upregulated PA expression (Fig. 5e and Fig. S22). The immunofluorescence staining images further verified the consistent trend for PA and PI (Fig. 5f). Overall, TLP can help to restrain the inflammatory response and reduce the fibrosis process, preventing postoperative tissue adhesion (Fig. 5g).

3.6. *Postoperative tissue antiadhesion in pigs*

Based on the excellent results obtained in the rat model, a pig model test was further performed to obtain reliable and superior results. Herein, common suture, commercial Coseal adhesive and the Interceed film that was approved by the Food and Drug Administration (FDA) in the United States served as the control group (Fig. 6a). During the surgical operation, Coseal hardly sealed the bleeding intestine due to weak adhesion (Movie S3). For Interceed, sutures must be used to help anchor the material to the pig intestine (Movie S4). The TLP adhered instantly and exhibited outstanding mechanical properties (Fig. S23, Movies S5 and S6).

csSupplementary video related to this article can be found at https://doi.org/10.1016/j.bioactmat.2022.12.003

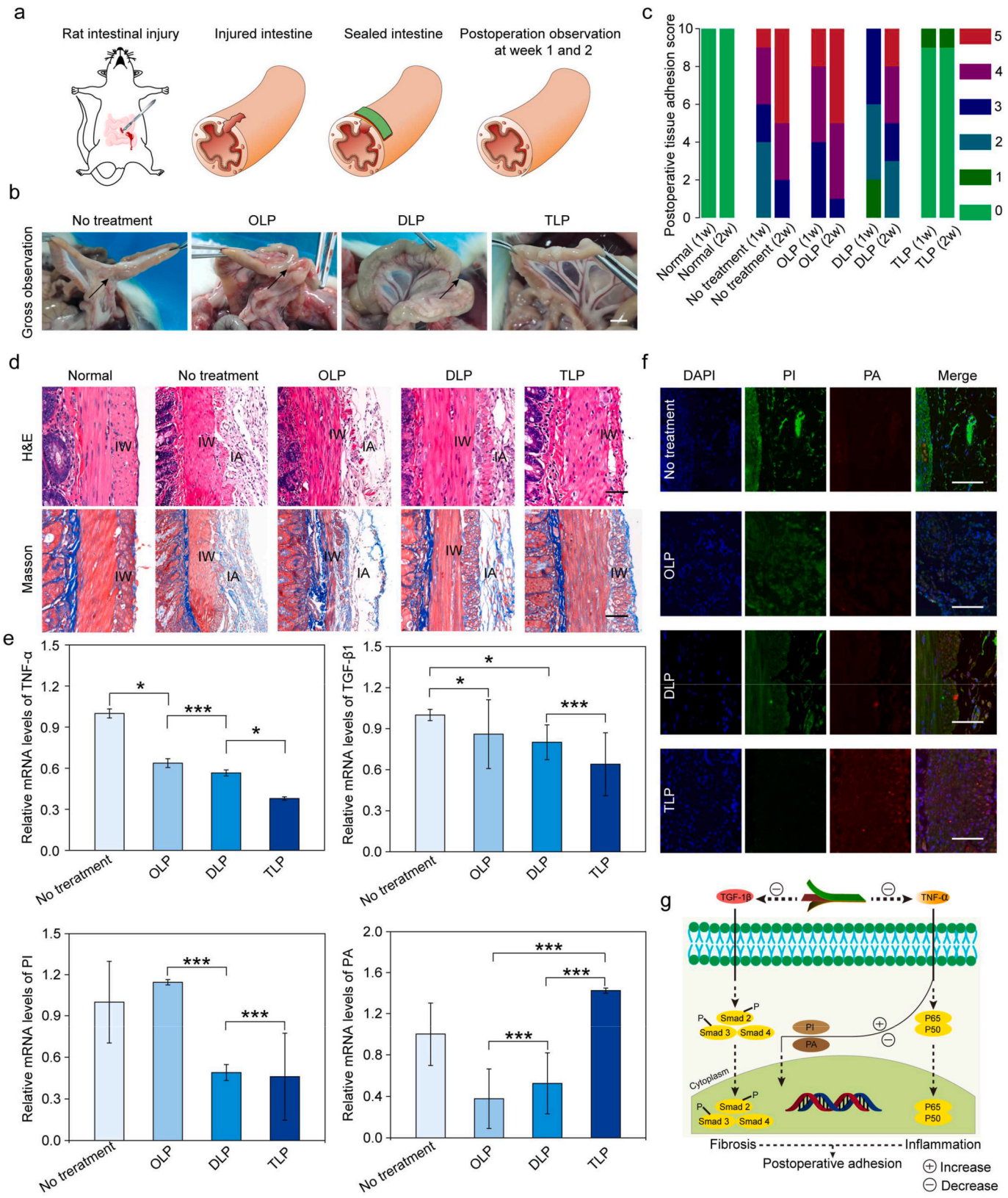

Fig. 5. *In vivo* tissue antiadhesion ability of the TLP. (a) Schematic diagram of the TLP for sealing intestinal injuries without postoperative tissue adhesion in an *in vivo* rat model. (b) Gross observation of the injured intestine sealed by the OLP, DLP and TLP. The no-treatment group was the control group. Scale bar: 1 cm. (c) Antiadhesion scores on day 14 postoperation. (d) Pathological analysis in the normal, no-treatment, OLP, DLP and TLP groups at 14 days postoperation. IW, intestine wall; IA, intestine adhesion. Scale bars: 100 μm. (e) The relative gene expression levels of transforming growth factor-β1 (TNF-β1), tumor necrosis factor-α (TNF-α), plasminogen activator inhibitor-1 (PI) and plasminogen activator (PA) in the injured intestine at 14 days postoperation (n = 5). PA reduces fibrosis, and PI promotes fibrosis. (f) Representative immunofluorescence staining at 14 days postoperation. Scale bars: 50 μm. (g) Molecular mechanism of TLP in preventing postoperative adhesions. $^{*}p < 0.05$, $^{***}p < 0.001$.

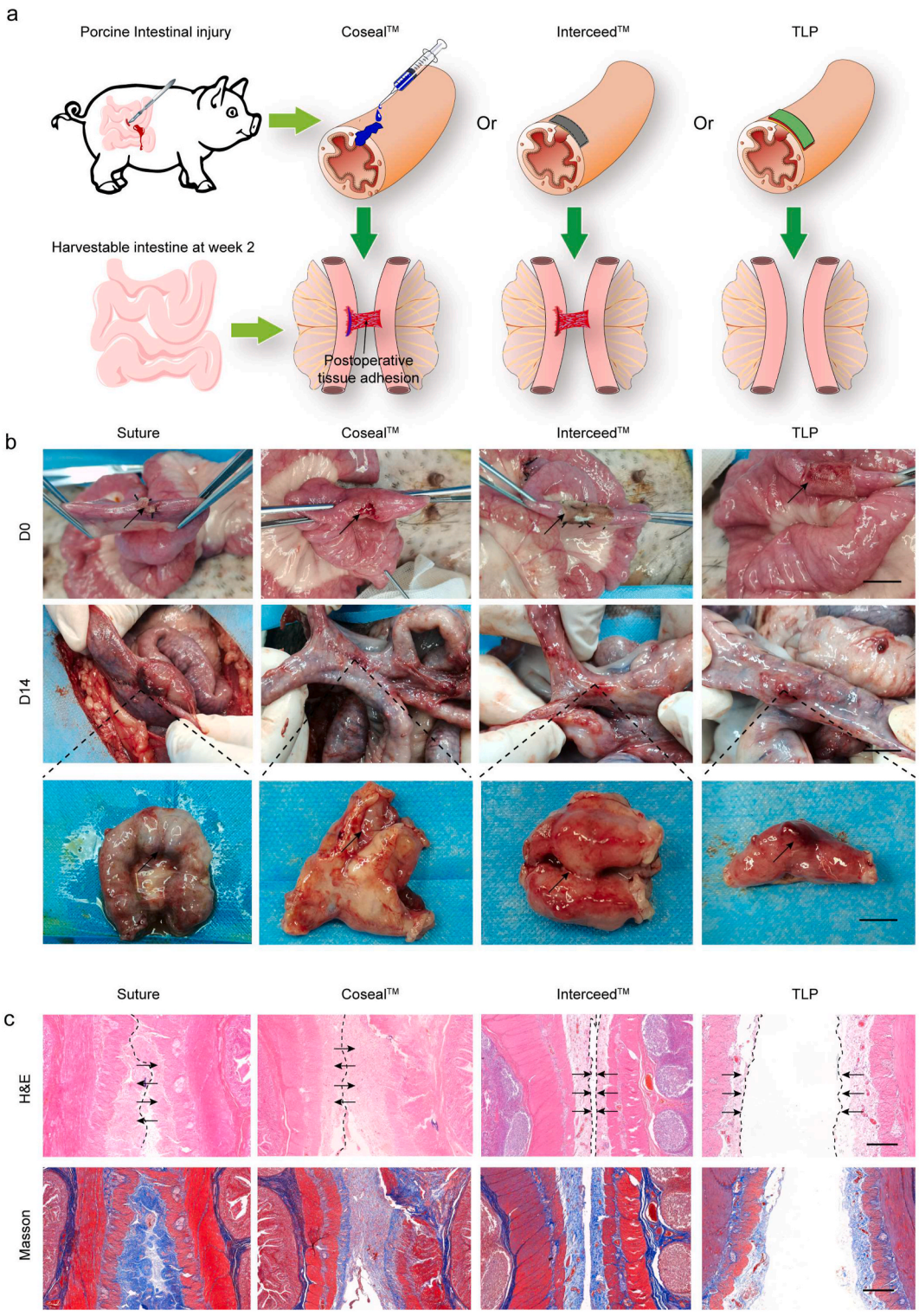

Fig. 6. Application and advantages of the TLP for effectively sealing intestinal injuries in a pig model. (a) Schematic illustrations of a pig intestine injury that was created and sealed by different materials to assess the adhesion and postoperative antiadhesion performance of the TLP. (b) Gross observation of the injured intestine that was sealed by sutures, commercial Coseal, Interceed and the prepared TLP on day 14. The black arrows indicate the surgical position. Scale bars: 2 cm. (c) Pathological analysis of specimens in the suture, commercial Coseal, Interceed and prepared TLP groups. The intact mesothelial layer is labeled with black arrows. Scale bars: 100 μm.

Two weeks after surgery, visual postoperative tissue adhesions formed in the suture and Coseal groups (Fig. 6b and Fig. S24a). The commercial film treatment slightly relieved tissue adhesion. No obvious tissue adhesion could be observed in the TLP group, which showed the best repair state (Fig. S24b). H&E analysis revealed that new tissue was connected with the injured intestine and surrounding tissue in the suture and Coseal groups. The TLP group had complete and normal tissue structures with clear and wide spaces (Fig. 6c). Moreover, Masson staining was performed, and through the observations, it was determined that the suture and Coseal groups had abundant collagen

depositions on their adhesion tissues, indicating that abundant fibroblast adhesion had occurred. Overall, the TLP exhibited a successive sealing capacity and excellent ability to prevent postoperative adhesion.

4. Conclusion

In summary, we report a versatile TLP patch system that is rationally designed with three functional components, including the inner adhesive matrix, middle reinforced layer and outer antiadhesive matrix. Through systematic in vitro tests, the TLP patch system was demonstrated to simultaneously combine a host of therapeutic functionalities, including instant wet adhesion to seal intestinal injury, a smooth outer surface to avoid unwanted tissue adhesion and biological inertness to inhibit cell and protein fouling. A middle layer matrix was utilized on the basis of a robust covalent effect and mechanical interlocking, providing intact structural stability and reinforced mechanical strength. Furthermore, this system exhibited superior biocompatibility compared to other systems, bioadhesion that was instant and resilient, and outstanding postoperative tissue antiadhesive performance. It was demonstrated in both rat and pig models that TLP can perfectly seal the injury without tissue adhesive obstacles. In addition, the sandwiched patches exhibited an outstanding ability to inhibit postoperative inflammation and fibrosis, as determined through molecular mechanism studies. Thus, this study established a potential therapeutic strategy for advancing the treatment of intestinal injuries.

Data availability

The data reported in this manuscript are available upon request.

Ethics approval and consent to participate

All animal experiments were performed in strict accordance with the Guide for the Care and Use of Laboratory Animals (Ministry of Science and Technology of the People's Republic of China, Policy No. 2006398). The animal procedures were performed in accordance with the Guidelines for Care and Use of Laboratory Animals of Huateng Biopharmaceutical Technology Co., LTD in Guangzhou, China and approved by the Animal Ethics Committee (approval No. HTSW210816).

CRediT authorship contribution statement

Wei Yang: Data curation, Methodology, Investigation, Writing – original draft. **Chengkai Xuan:** Methodology. **Xuemin Liu:** Investigation. **Qiang Zhang:** Investigation. **Kai Wu:** Methodology. **Liming Bian:** Writing – review & editing. **Xuetao Shi:** Supervision, Project administration, Funding acquisition, Writing – review & editing.

Declaration of competing interest

The authors have no conflicts to declare.

Acknowledgements

This work was financially supported by the National Key Research and Development Program of China (2021YFB3800800, 2018YFA0703000), the Science and Technology Program of Guangdong Province (2019B010941002), Science and Technology Program of Guangzhou (202206040001), the National Natural Science Foundation of China (32022041, U22A20157), the Key Research and Development Program of Guangzhou (20200702000, 22020B1515120075), and the Guangdong Basic and Applied Basic Research Foundation Outstanding Youth Project (2021B1515020064).

Appendix A. Supplementary data

Supplementary data to this article can be found online at https://doi.org/10.1016/j.bioactmat.2022.12.003.

References

[1] M. Honda, M. Kadohisa, D. Yoshii, Y. Komohara, T. Hibi, Directly recruited GATA6 + peritoneal cavity macrophages contribute to the repair of intestinal serosal injury, Nat. Commun. 12 (1) (2021) 7294.
[2] D. Zhong, D. Zhang, W. Chen, J. He, C. Ren, X. Zhang, N. Kong, W. Tao, M. Zhou, Orally deliverable strategy based on microalgal biomass for intestinal disease treatment, Sci. Adv. 7 (48) (2021), eabi9265.
[3] A. Zhao, H. Qin, M. Sun, M. Tang, J. Mei, K. Ma, X. Fu, Chemical conversion of human epidermal stem cells into intestinal goblet cells for modeling mucus-microbe interaction and therapy, Sci. Adv. 7 (16) (2021) eabb2213.
[4] M. Snelson, S.M. Tan, R.E. Clarke, C. de Pasquale, V. Thallas-Bonke, T.V. Nguyen, Processed foods drive intestinal barrier permeability and microvascular diseases, Sci. Adv. 7 (14) (2021), eabe4841.
[5] J. Wu, H. Yuk, T.L. Sarrafian, C.F. Guo, L.G. Griffiths, C.S. Nabzdyk, X. Zhao, An off-the-shelf bioadhesive patch for sutureless repair of gastrointestinal defects, Sci. Transl. Med. 14 (630) (2022), eabh2857.
[6] X. Peng, X. Xia, X. Xu, X. Yang, B. Yang, P. Zhao, W. Yuan, P.W.Y. Chiu, L. Bian, Ultrafast self-gelling powder mediates robust wet adhesion to promote healing of gastrointestinal perforations, Sci. Adv. 7 (23) (2021), eabe8739.
[7] S.Y. Yang, E.D. O'Cearbhaill, G.C. Sisk, K.M. Park, W.K. Cho, M. Villiger, B. E. Bouma, B. Pomahac, J.M. Karp, A bio-inspired swellable microneedle adhesive for mechanical interlocking with tissue, Nat. Commun. 4 (2013) 1702.
[8] Y. Hong, F. Zhou, Y. Hua, X. Zhang, C. Ni, D. Pan, Y. Zhang, D. Jiang, L. Yang, Q. Lin, Y. Zou, D. Yu, D.E. Arnot, X. Zou, L. Zhu, S. Zhang, H. Ouyang, A strongly adhesive hemostatic hydrogel for the repair of arterial and heart bleeds, Nat. Commun. 10 (1) (2019) 2060.
[9] E. Zhang, J. Yang, K. Wang, B. Song, H. Zhu, X. Han, Y. Shi, C. Yang, Z. Zeng, Z. Cao, Biodegradable zwitterionic cream gel for effective prevention of postoperative adhesion, Adv. Funct. Mater. 31 (10) (2021), 2009431.
[10] J. Yu, K. Wang, C. Fan, X. Zhao, J. Gao, W. Jing, X. Zhang, J. Li, Y. Li, J. Yang, W. Liu, An ultrasoft self-fused supramolecular polymer hydrogel for completely preventing postoperative tissue adhesion, Adv. Mater. 33 (16) (2021), e2008395.
[11] E. Zhang, B. Song, Y. Shi, H. Zhu, X. Han, H. Du, C. Yang, Z. Cao, Fouling-resistant zwitterionic polymers for complete prevention of postoperative adhesion, P. Natl. Acad. Sci. USA 117 (50) (2020) 32046–32055.
[12] S.O. Blacklow, J. Li, B.R. Freedman, M. Zeidi, C. Chen, D.J. Mooney, Bioinspired mechanically active adhesive dressings to accelerate wound closure, Sci. Adv. 5 (7) (2019), eaaw3963.
[13] J. Yang, R. Bai, B. Chen, Z. Suo, Hydrogel adhesion: a supramolecular synergy of chemistry, topology, and mechanics, Adv. Funct. Mater. 30 (2) (2019), 1901693.
[14] K. Zhang, X.M. Chen, Y. Xue, J.S. Lin, X.Y. Liang, J.J. Zhang, J. Zhang, G.D. Chen, C.C. Cai, J. Liu, Tough hydrogel bioadhesives for sutureless wound sealing, hemostasis and biointerfaces, Adv. Funct. Mater. 32 (15) (2021), 2111465.
[15] Y. Zhao, Y. Wu, L. Wang, M. Zhang, X. Chen, M. Liu, J. Fan, J. Liu, F. Zhou, Z. Wang, Bio-inspired reversible underwater adhesive, Nat. Commun. 8 (1) (2017) 2218.
[16] Z. Ma, G. Bao, J. Li, Multifaceted design and emerging applications of tissue adhesives, Adv. Mater. 33 (24) (2021), e2007663.
[17] H. Zhu, X. Mei, Y. He, H. Mao, W. Tang, R. Liu, J. Yang, K. Luo, Z. Gu, L. Zhou, Fast and high strength soft tissue bioadhesives based on a peptide dendrimer with antimicrobial properties and hemostatic ability, ACS Appl. Mater. Interfaces 12 (4) (2020) 4241–4253.
[18] G.M. Taboada, K. Yang, M.J.N. Pereira, S.S. Liu, Y. Hu, J.M. Karp, N. Artzi, Y. Lee, Overcoming the translational barriers of tissue adhesives, Nat. Rev. Mater. 5 (4) (2020) 310–329.
[19] M.C. Arno, M. Inam, A.C. Weems, Z. Li, A.L.A. Binch, C.I. Platt, S.M. Richardson, J. A. Hoyland, A.P. Dove, R.K. O'Reilly, Exploiting the role of nanoparticle shape in enhancing hydrogel adhesive and mechanical properties, Nat. Commun. 11 (1) (2020) 1420.
[20] N. Lang, M.J. Pereira, Y. Lee, I. Friehs, N.V. Vasilyev, E.N. Feins, K. Ablasser, E. D. O'Cearbhaill, C. Xu, A. Fabozzo, R. Padera, S. Wasserman, F. Freudenthal, L. S. Ferreira, R. Langer, J.M. Karp, P.J. del Nido, A blood-resistant surgical glue for minimally invasive repair of vessels and heart defects, Sci. Transl. Med. 6 (218) (2014) 218ra6.
[21] N. Annabi, Y.N. Zhang, A. Assmann, E.S. Sani, G. Cheng, A.D. Lassaletta, A. Vegh, B. Dehghani, G.U. Ruiz-Esparza, X. Wang, S. Gangadharan, A.S. Weiss, A. Khademhosseini, Engineering a highly elastic human protein-based sealant for surgical applications, Sci. Transl. Med. 9 (410) (2017) eaai7466.
[22] T. Wu, C. Cui, Y. Huang, Y. Liu, C. Fan, X. Han, Y. Yang, Z. Xu, B. Liu, G. Fan, W. Liu, Coadministration of an adhesive conductive hydrogel patch and an injectable hydrogel to treat myocardial infarction, ACS Appl. Mater. Interfaces 12 (2) (2020) 2039–2048.
[23] M.M. Hasani-Sadrabadi, P. Sarrion, S. Pouraghaei, Y. Chau, S. Ansari, S. Li, T. Aghaloo, A. Moshaverinia, An engineered cell-laden adhesive hydrogel promotes craniofacial bone tissue regeneration in rats, Sci. Transl. Med. 12 (534) (2020), eaay6853.

[24] H. Yuk, C.E. Varela, C.S. Nabzdyk, X. Mao, R.F. Padera, E.T. Roche, X. Zhao, Dry double-sided tape for adhesion of wet tissues and devices, Nature 575 (7781) (2019) 169–174.
[25] W. Zhang, B. Bao, F. Jiang, Y. Zhang, R. Zhou, Y. Lu, S. Lin, Q. Lin, X. Jiang, L. Zhu, Promoting oral mucosal wound healing with a hydrogel adhesive based on a phototriggered S-Nitrosylation coupling reaction, Adv. Mater. 33 (48) (2021), e2105667.
[26] C.Y. Cui, T.L. Wu, X.Y. Chen, Y. Liu, Y. Li, Z.Y. Xu, C.C. Fan, W.G. Liu, A janus hydrogel wet adhesive for internal tissue repair and anti-postoperative adhesion, Adv. Funct. Mater. 30 (49) (2020), 2005689.
[27] Y. Wang, L. Shang, G. Chen, L. Sun, X. Zhang, Y. Zhao, Bioinspired structural color patch with anisotropic surface adhesion, Sci. Adv. 6 (4) (2020), eaax8258.
[28] E. Milanese, T. Brink, R. Aghababaei, J.F. Molinari, Emergence of self-affine surfaces during adhesive wear, Nat. Commun. 10 (1) (2019) 1116.
[29] B.P. Lee, S. Konst, Novel hydrogel actuator inspired by reversible mussel adhesive protein chemistry, Adv. Mater. 26 (21) (2014) 3415–3419.
[30] S. Jiang, Z. Cao, Ultralow-fouling, functionalizable, and hydrolyzable zwitterionic materials and their derivatives for biological applications, Adv. Mater. 22 (9) (2010) 920–932.
[31] R. Calcutt, R. Vincent, D. Dean, T.L. Arinzeh, R. Dixit, Plant cell adhesion and growth on artificial fibrous scaffolds as an in vitro model for plant development, Sci. Adv. 7 (43) (2021), eabj1469.
[32] K. Hennig, I. Wang, P. Moreau, L. Valon, S. DeBeco, M. Coppey, Y.A. Miroshnikova, C. Albiges-Rizo, C. Favard, R. Voituriez, M. Balland, Stick-slip dynamics of cell adhesion triggers spontaneous symmetry breaking and directional migration of mesenchymal cells on one-dimensional lines, Sci. Adv. 6 (1) (2020), eaau5670.
[33] X. Lu, P.R. Nicovich, M. Zhao, D.J. Nieves, M. Mollazade, S.R.C. Vivekchand, K. Gaus, J.J. Gooding, Monolayer surface chemistry enables 2-colour single molecule localisation microscopy of adhesive ligands and adhesion proteins, Nat. Commun. 9 (1) (2018) 3320.
[34] L. Zhou, C. Dai, L. Fan, Y. Jiang, C. Liu, Z. Zhou, P. Guan, Y. Tian, J. Xing, X. Li, Y. Luo, P. Yu, C. Ning, G. Tan, Injectable self-healing natural biopolymer-based hydrogel adhesive with thermoresponsive reversible adhesion for minimally invasive surgery, Adv. Funct. Mater. 31 (14) (2021), 2007457.
[35] L. Teng, Y. Chen, M. Jin, Y. Jia, Y. Wang, L. Ren, Weak hydrogen bonds lead to self-healable and bioadhesive hybrid polymeric hydrogels with mineralization-active functions, Biomacromolecules 19 (6) (2018) 1939–1949.
[36] X.Y. He, L.Q. Liu, H.M. Han, W.Y. Shi, W. Yang, X.Q. Lu, Bioinspired and microgel-tackified adhesive hydrogel with rapid self-healing and high stretchability, Macromolecules 52 (1) (2019) 72–80.
[37] S. Hong, D. Pirovich, A. Kilcoyne, C.H. Huang, H. Lee, R. Weissleder, Supramolecular metallo-bioadhesive for minimally invasive use, Adv. Mater. 28 (39) (2016) 8675–8680.
[38] T. Chen, Y. Chen, H.U. Rehman, Z. Chen, Z. Yang, M. Wang, H. Li, H. Liu, Ultratough, self-healing, and tissue-adhesive hydrogel for wound dressing, ACS Appl. Mater. Interfaces 10 (39) (2018) 33523–33531.
[39] X. Jing, H.Y. Mi, Y.J. Lin, E. Enriquez, X.F. Peng, L.S. Turng, Highly stretchable and biocompatible strain sensors based on mussel-inspired super-adhesive self-healing hydrogels for human motion monitoring, ACS Appl. Mater. Interfaces 10 (24) (2018) 20897–20909.
[40] H. Jung, M.K. Kim, J.Y. Lee, S.W. Choi, J. Kim, Adhesive hydrogel patch with enhanced strength and adhesiveness to skin for transdermal Drug delivery, Adv. Funct. Mater. 30 (42) (2020), 2004407.
[41] L. Wang, X.H. Zhang, K. Yang, Y.V. Fu, T.S. Xu, S.L. Li, D.W. Zhang, L.N. Wang, C. S. Lee, A novel double-crosslinking-double-network design for injectable hydrogels with enhanced tissue adhesion and antibacterial capability for wound treatment, Adv. Funct. Mater. 30 (1) (2020), 1904156.
[42] D. Gan, W. Xing, L. Jiang, J. Fang, C. Zhao, F. Ren, L. Fang, K. Wang, X. Lu, Plant-inspired adhesive and tough hydrogel based on Ag-Lignin nanoparticles-triggered dynamic redox catechol chemistry, Nat. Commun. 10 (1) (2019) 1487.
[43] B. Liu, Y. Wang, Y. Miao, X. Zhang, Z. Fan, G. Singh, X. Zhang, K. Xu, B. Li, Z. Hu, M. Xing, Hydrogen bonds autonomously powered gelatin methacrylate hydrogels with super-elasticity, self-heal and underwater self-adhesion for sutureless skin and stomach surgery and E-skin, Biomaterials 171 (2018) 83–96.
[44] X.J. Pei, H. Zhang, Y. Zhou, L.J. Zhou, J. Fu, Stretchable, self-healing and tissue-adhesive zwitterionic hydrogels as strain sensors for wireless monitoring of organ motions, Mater. Horiz. 7 (7) (2020) 1872–1882.
[45] B. Zhang, L. Jia, J. Jiang, S. Wu, T. Xiang, S. Zhou, Biomimetic microstructured hydrogels with thermal-triggered switchable underwater adhesion and stable antiswelling property, ACS Appl. Mater. Interfaces 13 (30) (2021) 36574–36586.
[46] Q. Liu, D. Tan, F. Meng, B. Yang, Z. Shi, X. Wang, Q. Li, C. Nie, S. Liu, L. Xue, Adhesion enhancement of micropillar array by combining the adhesive design from gecko and tree frog, Small 17 (4) (2021), e2005493.
[47] X. Chen, Z. Lin, Y. Feng, H. Tan, X. Xu, J. Luo, J. Li, Zwitterionic PMCP-modified polycaprolactone surface for tissue engineering: antifouling, cell adhesion promotion, and osteogenic differentiation properties, Small 15 (42) (2019), e1903784.
[48] T. Agarwal, N. Celikkin, M. Costantini, T.K. Maiti, P. Makvandi, Recent advances in chemically defined and tunable hydrogel platforms for organoid culture, Bio-Des Manuf. 4 (3) (2021) 641–674.
[49] T.S. Su, A. Zheng, L.Y. Cao, L.J. Peng, X. Wang, J. Wang, X.Z. Xin, X.Q. Jiang, Adhesion-enhancing coating embedded with osteogenesis-promoting PDA/HA nanoparticles for peri-implant soft tissue sealing and osseointegration, Bio-Des Manuf. 5 (2) (2022) 233–248.
[50] X. Zeng, Z.G. Guo, W.M. Liu, Recent advances in slippery liquid-infused surfaces with unique properties inspired by nature, Bio-Des Manuf. 4 (3) (2021) 506–525.
[51] K.K. Zheng, Q.H. Gu, D. Zhou, M.R. Zhou, L. Zhang, Recent progress in surgical adhesives for biomedical applications, Smart Mater. Med. 3 (2022) 41–65.
[52] M. Zhang, C.X. Li, S.H. Yang, J. Hirte, C.S. Zhao, Ultra-transparent slippery surface, Smart Mater. Med. 2 (2021) 38–45.
[53] P.C. Li, W.H. Cai, K.B. Wang, L. Zhou, J. Wang, Selenium-functionalized polycarbonate-polyurethane for sustained in situ generation of therapeutic gas for blood-contacting materials, Smart Mater. Med. 3 (2022) 361–373.
[54] D. Hong, H.C. Hung, K. Wu, X. Lin, F. Sun, P. Zhang, S. Liu, K.E. Cook, S. Jiang, Achieving ultralow fouling under ambient conditions via surface-initiated ARGET ATRP of carboxybetaine, ACS Appl. Mater. Interfaces 9 (11) (2017) 9255–9259.
[55] G. Li, G. Cheng, H. Xue, S. Chen, F. Zhang, S. Jiang, Ultra low fouling zwitterionic polymers with a biomimetic adhesive group, Biomaterials 29 (35) (2008) 4592–4597.
[56] Y. Li, G.H. Li, Y. Chen, X.T. Zhao, Y.T. Wang, J. Liu, Z. Li, Gradient modulus tissue adhesive composite for dynamic wound closure, Adv. Funct. Mater. (2022), 2207306.
[57] L. Cheng, Y. Wang, G. Sun, S. Wen, L. Deng, H. Zhang, W. Cui, Hydration-enhanced lubricating electrospun nanofibrous membranes prevent tissue adhesion, Research 2020 (2020), 4907185.
[58] L.M. Stapleton, A.N. Steele, H. Wang, H.L. Hernandez, A.C. Yu, Use of a supramolecular polymeric hydrogel as an effective post-operative pericardial adhesion barrier, Nat. Biomed. Eng. 3 (8) (2019) 611–620.
[59] J. Li, W. Xu, J. Chen, D. Li, K. Zhang, T. Liu, J. Ding, X. Chen, Highly bioadhesive polymer membrane continuously releases cytostatic and anti-inflammatory drugs for peritoneal adhesion prevention, ACS Biomater. Sci. Eng. 4 (6) (2018) 2026–2036.
[60] Q. Gao, L.J. Duan, X.R. Feng, W.G. Xu, Superiority of poly(L-lactic acid) microspheres as dermal fillers, Chin. Chem. Lett. 32 (1) (2021) 577–582.